ACS OMEGA

Article

Cite This: ACS Omega 2018, 3, 17789−17796

http://pubs.acs.org/journal/acsodf

Distinguishing Zigzag and Armchair Edges on Graphene Nanoribbons by X-ray Photoelectron and Raman Spectroscopies

Jungpil Kim,*[,†] Nodo Lee,[†] Young Hwan Min,[†] Seokhwan Noh,[†] Nam-Koo Kim,[†] Seokwon Jung,[†] Minho Joo,[†] and Yasuhiro Yamada*[,‡]

[†]Materials & Devices Advanced Research Institute, LG Electronics, 10, Magokjungang-ro, Gangseo-gu, Seoul 07796, Republic of Korea

[‡]Graduate School of Engineering, Chiba University, 1-33 Yayoi, Inage, Chiba 263-8522, Japan

Supporting Information

ABSTRACT: Graphene nanoribbons (GNRs) have recently emerged as alternative 2D semiconductors owing to their fascinating electronic properties that include tunable band gaps and high charge-carrier mobilities. Identifying the atomic-scale edge structures of GNRs through structural investigations is very important to fully understand the electronic properties of these materials. Herein, we report an atomic-scale analysis of GNRs using simulated X-ray photoelectron spectroscopy (XPS) and Raman spectroscopy. Tetracene with zigzag edges and chrysene with armchair edges were selected as initial model structures, and their XPS and Raman spectra were analyzed. Structurally expanded nanoribbons based on tetracene and chrysene, in which zigzag and armchair edges were combined in various ratios, were then simulated. The edge structures of chain-shaped nanoribbons composed only of either zigzag edges or armchair edges were distinguishable by XPS and Raman spectroscopy, depending on the edge type. It was also possible to distinguish planar nanoribbons consisting of both zigzag and armchair edges with zigzag/armchair ratios of 4:1 or 1:4, indicating that it is possible to analyze normally synthesized GNRs because their zigzag to armchair edge ratios are usually greater than 4 or less than 0.25. Our study on the precise identification of GNR edge structures by XPS and Raman spectroscopy provides the groundwork for the analysis of GNRs.

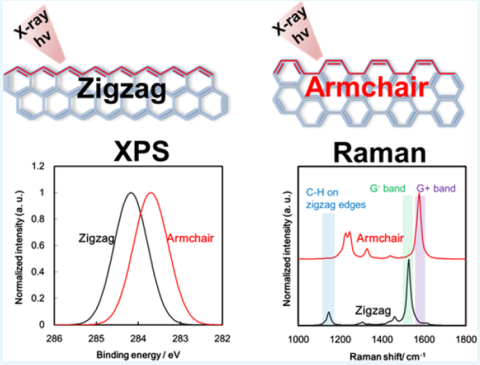

INTRODUCTION

Graphene nanoribbons (GNRs) have attracted attention as promising materials for nanosize electronics such as field-effect transistors.[1,2] GNRs have two basic edge structures, namely zigzag and armchair, and these edge structures have been intensively studied because the electronic and magnetic properties of GNRs depend on them.[3−9] GNRs with zigzag edges exhibit spin-polarized edge states with energies close to the Fermi level,[3−7] but GNRs with armchair edges have band gaps that are sensitive to the ribbon width.[7] The chemical properties of GNRs are also sensitive to the crystallographic orientations of their edges.[10−12] The reactivity of zigzag edges toward halogenation is greater than that of armchair edges because of the large number of electrons at the zigzag edges.[10]

Zigzag and armchair edges in GNRs synthesized by bottom-up fabrication have been observed by microscopic techniques such as scanning tunneling microscopy (STM).[13−15] For example, the edge electronic states have been directly observed by STM,[13−15] but long times are required for the analysis of edge positions. Moreover, probing the entire sample by atomic-scale microscopy is challenging; hence, it is necessary to develop other analytical techniques.

X-ray photoelectron spectroscopy (XPS) is a representative surface analysis method for determining the chemical composition and states of carbon materials.[16−24] Computational XPS has revealed defective carbon material structures such as sp^3C-sp^3C,[19] edge C−H,[20] functional groups,[21,22] vacancy defects,[23,24] and pentagonal and heptagonal rings[20,23,24] in graphene. Unfortunately, spectral differences between the zigzag and armchair edges in graphene have not been reported because the number of carbon atoms at the edges of graphene is negligible compared to that in its basal plane. However, it is essential to clarify the peak positions of zigzag and armchair edges in GNRs.

Raman spectroscopy is also among the most used methods for analyzing carbon materials because the presence of disorder in sp^2-carbon systems results in Raman spectral resonances.[25] Raman spectroscopy is commonly used to determine the number of layers, defect density, strain, thermal properties, and level of doping in graphene by examining its signature G, D, D′, and planar bands.[26−32] Moreover, the zigzag and armchair edges in graphene have been determined by Raman spectroscopy, which revealed that the D band of a zigzag edge is considerably less intense than that of an armchair edge.[25,33−36]

Received: October 10, 2018
Accepted: December 4, 2018
Published: December 19, 2018

DOI: 10.1021/acsomega.8b02744
ACS Omega 2018, 3, 17789−17796

In addition, several bands originating from the zigzag and armchair edges still need to be assigned.

In this work, C 1s XPS spectra of tetracene with zigzag edges and chrysene with armchair edges as well as their expanded structures were simulated using density functional theory (DFT). In addition, the Raman spectra of GNRs were simulated to determine the spectral differences between the zigzag and armchair edges. As a complementary experimental approach, tetracene, chrysene, and highly oriented pyrolytic graphite (HOPG) were analyzed by XPS and Raman spectroscopy.

RESULTS AND DISCUSSION

Electronic Properties. The difference between the electronic property of zigzag and armchair GNRs, such as the band gap, has been reported.[37−39] The reported band gaps of zigzag GNRs are smaller than those of armchair GNRs,[37] and the band gap increases with increasing size of the GNR.[38,39] Table 1 shows the band gaps for various GNRs with zigzag and armchair edges. In Table 1, chain structures with zigzag edges are abbreviated as "*ZN*," where "Z" refers to "zigzag" and *N* is the number of aromatic rings (Figure 1b). Similarly, "*AN*" refers to chains of armchair structures with N armchair edges (Figure 1b). Planar structures with zigzag and armchair edges (Figure 1c) are similarly referred to as "*ZX*-*AY*" or "*AX*-*ZY*" (Figure 1c). *X* and *Y* are the numbers of aromatic rings. Similar to the results of previous reports, GNRs based on Z8 have smaller band gaps than GNRs based on A8 of the same size. Moreover, the band gaps increase with increasing size of the GNRs.

Table 1. HOMO−LUMO Gaps of GNRs with Zigzag and Armchair Edges (HOMO = Highest Occupied Molecular Orbital and LUMO = Lowest Unoccupied Molecular Orbital)

model	HOMO−LUMO gap (eV)	model	HOMO−LUMO gap (eV)
Z8	1.00	A8	3.45
Z8-A2	0.83	A8-Z2	2.47
Z8-A4	0.23	A8-Z4	0.84
Z8-A6	0.10	A8-Z6	0.18

X-ray Photoelectron Spectroscopy. Tetracene, chrysene, and HOPG were analyzed by XPS, and their XPS C 1s spectra are shown in Figure 2a. The binding energy of the C 1s spectral peak of each sample was obtained after adjusting the energy of the valence band edge to 0 eV (Figure 2b). The full width at half-maximum values are listed in Table S1 in the Supporting Information. The spectra reveal the lack of C 1s peak shifts due to adsorbed oxygen atoms, considering the number of oxygen atoms on tetracene, chrysene, and HOPG (Figure S1). Tetracene and chrysene were examined thrice at identical positions to confirm that the X-ray beam did not damage the samples; indeed, no peak changes were observed (Figure S2).

Interestingly, the C 1s peaks of tetracene with zigzag edges and chrysene with armchair edges appeared at 283.9 and 283.3 eV, respectively (Figure 2a), although tetracene and chrysene contain identical number of carbon and hydrogen atoms (Figure 1). Moreover, this difference between the peak positions of tetracene and chrysene was also observed in the simulated XPS spectra (Figure 3a−c), indicating that the C 1s peak is positioned at a higher binding energy in the zigzag edge case. The analogous peak in the spectrum of HOPG was observed at 284.3 eV (Figure 2a). The differences in the peak positions of the various samples can be explained by their work functions, which were calculated in this study to be 4.87, 5.53, and 3.76 eV for Z4 (tetracene), A4 (chrysene), and Z8-A8, respectively, from the energy differences between the HOMO levels and the vacuum level[20] (Figure 1). The binding energies were observed to decrease with increasing work function value as the valence band edge approached the atomic nuclei.[20]

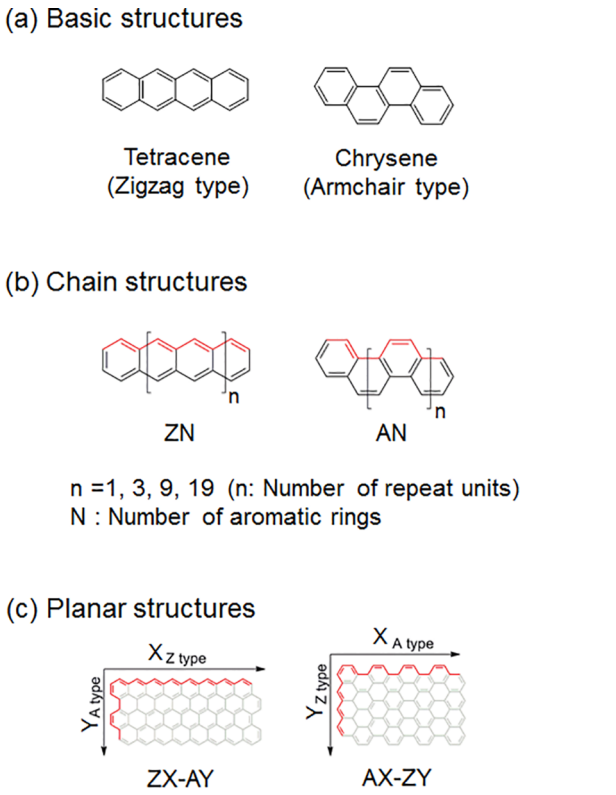

Figure 1. Model structures with zigzag and armchair edges: (a) basic structures, (b) chain structures, and (c) planar structures. Terminating hydrogen atoms are omitted.

Having acquired and simulated the XPS spectra of tetracene, chrysene, and HOPG (Figures 2 and 3), the spectra of expanded aromatic hydrocarbons with zigzag and armchair edges were next simulated (Figures 1 and 3). To determine how the peak positions in the spectra depend on the edge structure, we simulated the XPS spectra of the expanded chain structures, which are large-sized structures without conjugated carbons in their basal planes (Figure 3a−c). In the chain structures based on tetracene (Figures 1b and 3a), the C 1s peak observed at 283.9 eV for Z4 was slightly shifted to 284.2 eV in the spectrum of Z20, but the energy of this peak did not change further as the number of benzene rings was increased, as in Z40. These results show that the C 1s peaks do not undergo any extreme shifts in this system.

In the chain structures based on chrysene (Figures 1b and 3b), the C 1s peak observed at 283.3 eV for A4 shifted slightly to 283.4 eV in the spectrum of A8, but this peak energy exhibited no further change with increasing number of benzene rings (A20 and A40). Figure 3c reveals that the difference in the Z4 and A4 C 1s peak energies is 0.6 eV, with values of 0.7

DOI: 10.1021/acsomega.8b02744
ACS Omega 2018, 3, 17789−17796

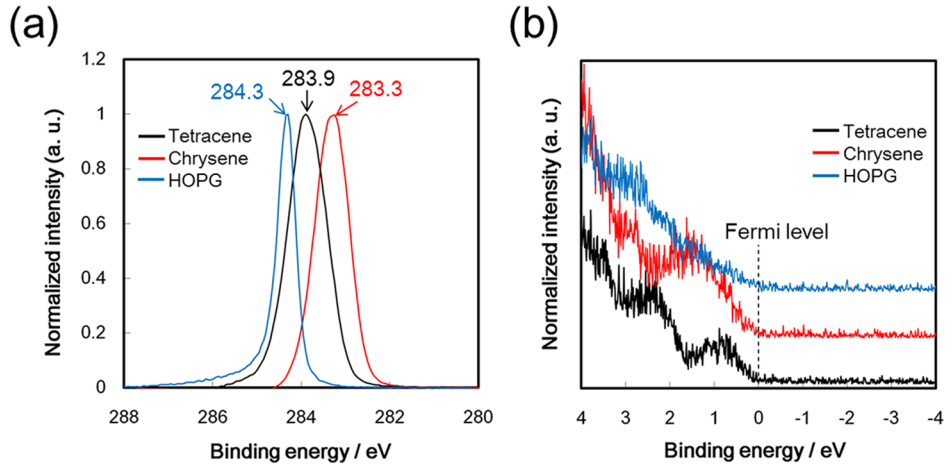

Figure 2. Experimental XPS spectra acquired for tetracene, chrysene, and HOPG: (a) XPS C 1s spectra and (b) XPS spectra at the valence band edge.

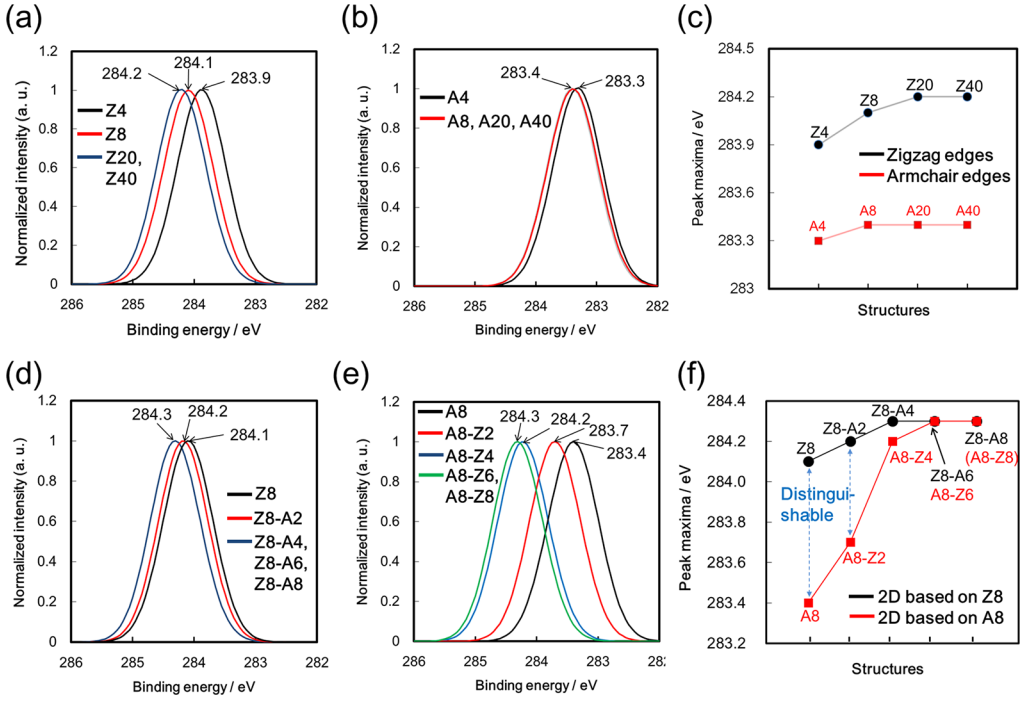

Figure 3. Simulated XPS C 1s spectra of the expanded aromatic hydrocarbons with zigzag and armchair edges shown in Figure 1. Spectra of chain structures based on (a) tetracene and (b) chrysene. (c) Spectral peak shifts of chain structures based on tetracene and chrysene. Spectra of planar structures based on (d) Z8 and (e) A8. (f) Spectral peak shifts of planar structures based on Z8 and A8.

eV (Z8/A8), 0.8 eV (Z20/A20), and 0.8 eV (Z40/A40) for the remaining differences, which demonstrates that the zigzag and armchair edges in these chain structures are distinguishable by XPS.

Figures 1c and 3d reveal that the peak observed for Z8 (284.1 eV) shifted to 284.3 eV as the number of tiers was increased to Z8-A4, but no further shift was observed upon the inclusion of additional tiers. Similarly, Figures 1c and 3e reveal that the peak corresponding to A8 (283.4 eV) shifted to 284.3 eV as the number of tiers was increased to A8-Z6, but no further shift was observed upon the inclusion of additional tiers. The observed peak shifts to higher binding energies with increasing number of tiers are ascribable to increments in the number of conjugated carbons in the basal plane.

Comparison of the spectra of the planar Z8- and A8-based structures (Figure 3f) reveals the difference between the Z8 and A8 C 1s peak energies to be 0.7 eV and that between Z8-A2 and A8-Z2 to be 0.5 eV. These results reveal that GNR structures can be distinguished by XPS because the peaks in the spectra of Z8-A2 (zigzag/armchair = 4:1) and A8-Z2 (zigzag/armchair = 1:4) are observed at different energy values. However, these differences decrease as the structures are expanded in planar directions (Figure 3f) because the number of carbon atoms on the edges is negligible compared to that in the basal planes. For example, the C 1s peaks for Z8-A4 and A8-Z4 are separated by 0.1 eV, whereas those for Z8-A6 and A8-Z6 are identical (0 eV difference) (Figure 3f).

Raman Spectroscopy. Figure 4 shows the experimental and simulated Raman spectra of tetracene and chrysene; the

DOI: 10.1021/acsomega.8b02744
ACS Omega 2018, 3, 17789−17796

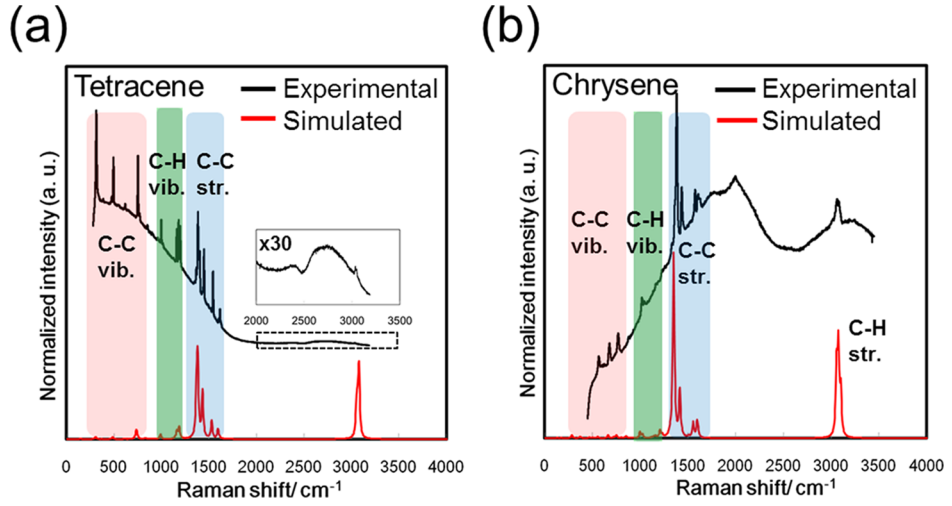

Figure 4. Experimental and simulated Raman spectra: (a) tetracene and (b) chrysene.

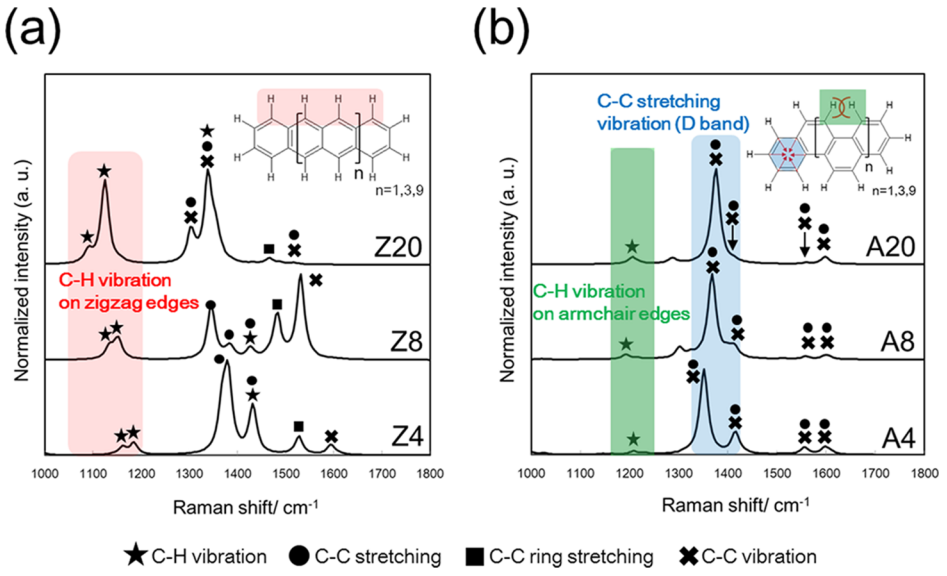

Figure 5. Simulated Raman spectra of the chain-shaped GNRs with zigzag and armchair edges shown in Figure 1b: (a) zigzag edges and (b) armchair edges.

experimental spectra were obtained at a laser excitation wavelength of 785 nm because background fluorescence emissions can occur at shorter laser wavelengths such as 514 and 633 nm.[40] Tables S2 and S3 summarize the peak assignments for the Raman spectra of tetracene and chrysene, respectively; all peaks in the experimental spectra were assigned by observing their vibrational modes (Movies, Supporting Information).

The experimental Raman spectrum of tetracene (Figure 4a and Table S2) shows peaks at 997, 1179, and 1196 cm^{-1} that originate from C−H bending vibrations, whereas the peaks at 1383, 1447, 1541, and 1615 cm^{-1} are assigned to C−C stretching, C−C stretching vibration, C−C ring stretching, and C−C vibration, respectively; the peak at 3077 cm^{-1} is due to C−H stretching. The experimental Raman spectrum of chrysene (Figure 4b and Table S3) shows peaks at 1018 and 1230 cm^{-1} that correspond to C−H bending vibrations, whereas the peaks at 1380, 1434, 1576, and 1621 cm^{-1} are assigned to various C−C stretching vibrations; the peak at 3060 cm^{-1} is due to C−H stretching. Detailed peak assignments are provided in Tables S1 and S2 and Movies (Supporting Information). The peaks in the simulated Raman spectra match well with those in the experimental Raman spectra (Figure 4 and Tables S1 and S2).

With these Raman spectra as references, the spectra of the expanded aromatic hydrocarbons with zigzag and armchair edges were simulated (Figures 1 and S3). Because only peaks in the 1000−1800 cm^{-1} Raman shift range are distinguishable in the simulated spectra on the basis of the edge structure (Figure S3), only spectra in this range were analyzed in detail (Figure 5 and Movies).

Several peaks originating from C−H and C−C vibrations are evident in the spectra of the chain structures with zigzag edges (Figure 5a). In particular, the intensities of the peaks at 1161 and 1180 cm^{-1} that originate from C−H bending vibrations on zigzag edges in the Raman spectrum of Z4 were observed to increase with increasing number of zigzag edges (Figure 5a and Movies). Weak peaks at 1206 cm^{-1}, which correspond to C−H vibrations on armchair edges, are observed in the spectra of the chain structures with armchair edges (Figure 5b and Movies),

DOI: 10.1021/acsomega.8b02744
ACS Omega 2018, 3, 17789−17796

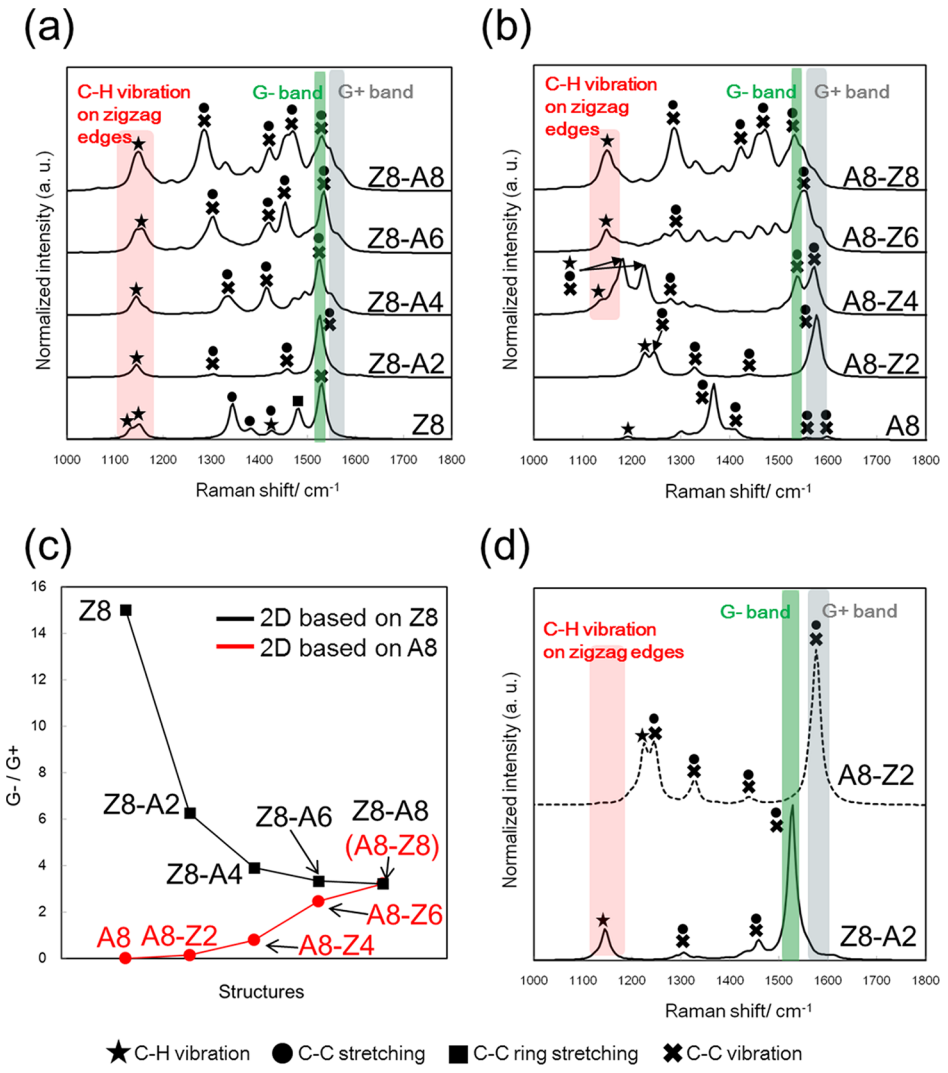

Figure 6. Simulated Raman spectra of the planar GNRs with zigzag and armchair edges shown in Figure 1c. Planar structures based on (a) Z8 and (b) A8. (c) Values of G^-/G^+. (d) Simulated Raman spectra of Z8-A2 and A8-Z2.

which are also evident in the experimental spectra of tetracene and chrysene (Figure 4); these peaks are weak because of steric barriers that hinder C−H vibrations along the armchair edges, as shown in the molecular structure in Figure 5b. These results reveal that C−H vibrations correspond to strong peaks when the C−H units are present on zigzag edges (Figure 4). The peak at 1350 cm^{-1} was intense (rather than that associated with C−H vibrations) in the spectra of chain structures with armchair edges (Figures 1a and 5b);[25,33−35] this peak corresponds to C−C stretching vibrations in chain structures with armchair edges (Figure 5b and Movies) and is referred to as the "D band." These spectra reveal that the zigzag and armchair edges in the chain structures are distinguishable by Raman spectroscopy as well as XPS.

Peaks that correspond to C−H and C−C vibrations are more apparent in the Raman spectra of the planar structures based on Z8 (Figures 1c and 6a) and A8 (Figures 1c and 6b) than those in the spectra of the corresponding chain structures, which is ascribable to their more complicated structures. Among the various peaks, the ratio of zigzag to armchair edges was determined using two peaks, one that corresponds to C−H vibrations on zigzag edges and the other that corresponds to C−C stretching vibrations, as well as Raman analysis for chain structures. Other vibrational modes are listed in the Movie in the Supporting Information. Peaks at ∼1150 cm^{-1} that correspond to C−H bending on zigzag edges are evident in the spectra of the planar structures based on Z8, such as Z8, Z8-A2, Z8-A4, Z8-A6, and Z8-A8 (Figure 6a), as well as structures based on A8, such as A8-Z4, Z8-Z6, and A8-Z8 (Figure 6b). Although the position of this peak was not very sensitive to the structure, the peak due to C−C stretching was dramatically affected; for example, the C−C peak at 1350 cm^{-1} in the spectra of the chain structures with armchair edges (Figure 5b) did not appear at that position in the planar structures based on Z8 (Figures 1c and 6a) and A8 (Figures 1c and 6b). This observation is ascribable to C−C structures that change with the changing basal plane structure, whereas the C−H-edge structures are unaffected by changes in the structure of the basal plane.

The G band is considered to be a typical peak in the Raman spectrum of a nanocarbon material, and it is divided into G^- and G^+ bands for carbon nanotubes, depending on the structure of the nanotube. Similar separation of G^- and G^+ bands in the Raman spectra of zigzag GNRs has also been reported.[41] The G^- band and G^+ bands originate from the zigzag edges and the basal plane of zigzag GNRs, respectively,

DOI: 10.1021/acsomega.8b02744
ACS Omega 2018, 3, 17789−17796

and the $I(G^+)/I(G^-)$ ratio [here, $I(G^+)$ and $I(G^-)$ represent the intensities of the G^- and G^+ bands, respectively] increases with increasing width of zigzag GNRs. We also observed a similar phenomenon in the spectra of the planar structures based on Z8 and A8 (Figure 6); a G^- band was observed in Z8, whereas the intensity of the G^+ band increased with increasing number of armchair edges (Figure 6a,c). In contrast, the intensity of the G^- band increased with increasing number of zigzag edges in A8 (Figure 6b,c). Clearly, the spectra of Z8-A2 (zigzag/armchair = 4:1) and A8-Z2 (zigzag/armchair = 1:4) can be used to distinguish these structures by determining the presence or absence of G^- or G^+ bands (Figure 6d). Moreover, these structures can also be distinguished by the presence of the peak corresponding to C−H vibrations in zigzag edges (Figure 6d). A peak at 1145 cm^{-1} was observed in the spectrum of Z8-A2, but this peak was absent in the spectrum of A8-Z2, which indicates that the structures of normally synthesized GNRs can also be determined by Raman spectroscopy because the ratio of zigzag to armchair edges in normally synthesized GNRs is usually greater than 4 or less than 0.25.

CONCLUSIONS

We investigated GNRs with zigzag and armchair edges using XPS and Raman spectroscopy by first examining chain-shaped GNRs with only zigzag or armchair edges. The difference between the C 1s binding energies of tetracene and chrysene was determined by XPS to be 0.6 eV, whereas that between GNRs with zigzag edges and armchair edges was higher, at 0.8 eV. Raman spectroscopy revealed that a strong peak at ∼1170 cm^{-1}, which corresponds to C−H bending vibrations on zigzag edges, appeared in the spectra of GNRs with zigzag edges; however this peak was absent in the spectra of GNRs with armchair edges. Instead, a strong peak at ∼1350 cm^{-1} corresponding to C−C stretching vibrations was observed in the spectra of GNRs with armchair edges. These results indicate that the zigzag and armchair edges in chain structures are distinguishable by XPS and Raman spectroscopy. On the basis of the analyses of the spectra of chain-shaped GNRs, the spectra of planar GNRs with zigzag and armchair edges were estimated. XPS revealed that the difference in the C 1s binding energies of zigzag-rich GNRs (zigzag/armchair = 4:1) and armchair-rich GNRs (zigzag/armchair = 1:4) is 0.5 eV, which indicates that these peaks are spectrally distinguishable. The zigzag-rich (zigzag/armchair = 4:1) and armchair-rich (zigzag/armchair = 1:4) GNRs could also be distinguished by Raman spectroscopy by determining the presence of G^- or G^+ bands as well as peaks that correspond to C−H vibrations on zigzag edges. These results indicate that planar GNRs can also be distinguished by XPS and Raman spectroscopy depending on the ratio of zigzag to armchair edges. This improved understanding of the XPS and Raman spectroscopy of GNRs with zigzag and armchair edges may lead to the structural optimization of GNRs for nanosized electronic device applications.

EXPERIMENTAL SECTION

Experimental Spectroscopy. Polycyclic aromatic hydrocarbons, viz., tetracene (98%, Tokyo Chemical Industry Co., Ltd.), chrysene (98%, Sigma-Aldrich Co., Ltd.), and HOPG (SPI-1 Grade, SPI Supplies), were analyzed by XPS and Raman spectroscopy. To avoid sample oxidation, the spectra were acquired soon after opening the purchased sample bottles.

XPS (ESCALAB 250Xi, Thermo Fisher Scientific Inc.) was conducted at a pass energy of 10 eV using an Al Kα X-ray gun at 10 mA and 15 kV. Each sample was placed on a conductive copper tape and then pressed. A flood gun was used to neutralize the charge. The C 1s signals in each spectrum were normalized against the signal of highest intensity. Raman spectroscopy (NRS 3200, JASCO Corp.) was conducted using a Raman spectrometer equipped with a CCD detector cooled with a Peltier-type cooling system. The 785 nm line of a ∼40 mW Nd/YAG laser was used for Raman excitation.

Computational Spectroscopy. Tetracene with zigzag edges and chrysene with armchair edges were used as the initial structures in this study (Figure 1a). To determine the spectral differences between zigzag and armchair edges, we built chain structures with zigzag and armchair edges, as shown in Figure 1b. The ground-state geometry was fully optimized on the B3LYP/6-31G(d,p) level in the gas phase. From the optimized geometry, the vertical singlet−singlet electronic transition energies were calculated via the time-dependent DFT method. XPS spectra were simulated using population analyses performed on the B3LYP/6-31g(d) level to calculate the electronic energy levels; detailed procedures are provided in the Supporting Information and other papers.[20−22,42] Raman spectra were generated from the optimized structures by vibrational frequency calculations. All B3LYP/6-31g(d)-calculated frequencies were scaled by 0.96. The Gaussian 09[43] quantum chemistry software package was used for all calculations.

ASSOCIATED CONTENT

Supporting Information

The Supporting Information is available free of charge on the ACS Publications website at DOI: 10.1021/acsomega.8b02744.

Details on XPS spectral simulation, XPS spectra, and Raman spectra (PDF)

Raman vibration (ZIP)

AUTHOR INFORMATION

Corresponding Authors

*E-mail: jp.kim@lge.com. Phone/Fax: +82-2-6987-1671 (J.K.).

*E-mail: y-yamada@faculty.chiba-u.jp. Phone/Fax: +81-43-290-3376 (Y.Y.).

ORCID

Jungpil Kim: 0000-0003-3663-2774

Yasuhiro Yamada: 0000-0002-4974-5148

Notes

The authors declare no competing financial interest.

ACKNOWLEDGMENTS

The authors are grateful for the assistance of Dr. Jeong Soo Lee (Head of Materials & Devices Advanced Research Institute).

REFERENCES

(1) Li, X.; Wang, X.; Zhang, L.; Lee, S.; Dai, H. Chemically derived, ultrasmooth graphene nanoribbon semiconductors. *Science* **2008**, *319*, 1229−1232.

(2) Wang, X.; Ouyang, Y.; Li, X.; Wang, H.; Guo, J.; Dai, H. Room-temperature all-semiconducting sub-10-nm graphene nanoribbon field-effect transistors. *Phys. Rev. Lett.* **2008**, *100*, 206803.
(3) Nakada, K.; Fujita, M.; Dresselhaus, G.; Dresselhaus, M. S. Edge state in graphene ribbons: Nanometer size effect and edge shape dependence. *Phys. Rev. B: Condens. Matter Mater. Phys.* **1996**, *54*, 17954.
(4) Wakabayashi, K.; Fujita, M.; Ajiki, H.; Sigrist, M. Electronic and magnetic properties of nanographite ribbons. *Phys. Rev. B: Condens. Matter Mater. Phys.* **1999**, *59*, 8271.
(5) Yazyev, O. V. Emergence of magnetism in graphene materials and nanostructures. *Rep. Prog. Phys.* **2010**, *73*, 056501.
(6) Son, Y.-W.; Cohen, M. L.; Louie, S. G. Half-metallic graphene nanoribbons. *Nature* **2007**, *446*, 342.
(7) Kimouche, A.; Ervasti, M. M.; Drost, R.; Halonen, S.; Harju, A.; Joensuu, P. M.; Sainio, J.; Liljeroth, P. Ultra-narrow metallic armchair graphene nanoribbons. *Nat. Commun.* **2015**, *6*, 10177.
(8) Wassmann, T.; Seitsonen, A. P.; Saitta, A. M.; Lazzeri, M.; Mauri, F. Structure, stability, edge states, and aromaticity of graphene ribbons. *Phys. Rev. Lett.* **2008**, *101*, 096402.
(9) Neto, A. H. C.; Guinea, F.; Peres, N. M. R.; Novoselov, K. S.; Geim, A. K. The electronic properties of graphene. *Rev. Mod. Phys.* **2009**, *81*, 109.
(10) Kim, J.; Yamada, Y.; Fujita, R.; Sato, S. Bromination of graphene with pentagonal, hexagonal zigzag and armchair, and heptagonal edges. *J. Mater. Sci.* **2015**, *50*, 5183−5190.
(11) Boukhvalov, D. W.; Katsnelson, M. I. Chemical functionalization of graphene with defects. *Nano Lett.* **2008**, *8*, 4373−4379.
(12) Seitsonen, A. P.; Saitta, A. M.; Wassmann, T.; Lazzeri, M.; Mauri, F. Structure and stability of graphene nanoribbons in oxygen, carbon dioxide, water, and ammonia. *Phys. Rev. B: Condens. Matter Mater. Phys.* **2010**, *82*, 115425.
(13) Cai, J.; Ruffieux, P.; Jaafar, R.; Bieri, M.; Braun, T.; Blankenburg, S.; Muoth, M.; Seitsonen, A. P.; Saleh, M.; Feng, X. Atomically precise bottom-up fabrication of graphene nanoribbons. *Nature* **2010**, *466*, 470.
(14) Han, P.; Akagi, K.; Federici Canova, F.; Mutoh, H.; Shiraki, S.; Iwaya, K.; Weiss, P. S.; Asao, N.; Hitosugi, T. Bottom-up graphene-nanoribbon fabrication reveals chiral edges and enantioselectivity. *ACS Nano* **2014**, *8*, 9181−9187.
(15) Vo, T. H.; Shekhirev, M.; Kunkel, D. A.; Orange, F.; Guinel, M. J.-F.; Enders, A.; Sinitskii, A. Bottom-up solution synthesis of narrow nitrogen-doped graphene nanoribbons. *Chem. Commun.* **2014**, *50*, 4172−4174.
(16) Ishitani, A. Application of X-ray photoelectron spectroscopy to surface analysis of carbon fiber. *Carbon* **1981**, *19*, 269−275.
(17) Proctor, A.; Sherwood, P. M. A. X-ray photoelectron spectroscopic studies of carbon fibre surfaces. I. carbon fibre spectra and the effects of heat treatment. *J. Electron Spectrosc. Relat. Phenom.* **1982**, *27*, 39−56.
(18) Boutique, J. P.; Verbist, J. J.; Fripiat, J. G.; Delhalle, J.; Pfister-Guillouzo, G.; Ashwell, G. J. 3,5,11,13-Tetraazacycl[3.3.3]azine: theoretical (ab initio) and experimental (x-ray and ultraviolet photoelectron spectroscopy) studies of the electronic structure. *J. Am. Chem. Soc.* **1984**, *106*, 4374−4378.
(19) Fujimoto, A.; Yamada, Y.; Koinuma, M.; Sato, S. Origins of sp3C peaks in C1s X-ray Photoelectron Spectra of Carbon Materials. *Anal. Chem.* **2016**, *88*, 6110−6114.
(20) Kim, J.; Yamada, Y.; Kawai, M.; Tanabe, T.; Sato, S. Spectral change of simulated X-ray photoelectron spectroscopy from graphene to fullerene. *J. Mater. Sci.* **2015**, *50*, 6739−6747.
(21) Yamada, Y.; Kim, J.; Matsuo, S.; Sato, S. Nitrogen-containing graphene analyzed by X-ray photoelectron spectroscopy. *Carbon* **2014**, *70*, 59−74.
(22) Yamada, Y.; Yasuda, H.; Murota, K.; Nakamura, M.; Sodesawa, T.; Sato, S. Analysis of heat-treated graphite oxide by X-ray photoelectron spectroscopy. *J. Mater. Sci.* **2013**, *48*, 8171−8198.
(23) Susi, T.; Kaukonen, M.; Havu, P.; Ljungberg, M. P.; Ayala, P.; Kauppinen, E. I. Core level binding energies of functionalized and defective graphene. *Beilstein J. Nanotechnol.* **2014**, *5*, 121.
(24) Barinov, A.; Malcioğlu, O. B.; Fabris, S.; Sun, T.; Gregoratti, L.; Dalmiglio, M.; Kiskinova, M. Initial stages of oxidation on graphitic surfaces: photoemission study and density functional theory calculations. *J. Phys. Chem. C* **2009**, *113*, 9009−9013.
(25) Ferrari, A. C.; Basko, D. M. Raman spectroscopy as a versatile tool for studying the properties of graphene. *Nat. Nanotechnol.* **2013**, *8*, 235−246.
(26) Cançado, L. G.; Pimenta, M.; Neves, B.; Dantas, M.; Jorio, A. Influence of the atomic structure on the Raman spectra of graphite edges. *Phys. Rev. Lett.* **2004**, *93*, 247401.
(27) Ferrari, A. C.; Meyer, J.; Scardaci, V.; Casiraghi, C.; Lazzeri, M.; Mauri, F.; Piscanec, S.; Jiang, D.; Novoselov, K.; Roth, S. Raman spectrum of graphene and graphene layers. *Phys. Rev. Lett.* **2006**, *97*, 187401.
(28) Das, A.; Pisana, S.; Chakraborty, B.; Piscanec, S.; Saha, S. K.; Waghmare, U. V.; Novoselov, K. S.; Krishnamurthy, H. R.; Geim, A. K.; Ferrari, A. C.; Sood, A. K. Monitoring dopants by Raman scattering in an electrochemically top-gated graphene transistor. *Nat. Nanotechnol.* **2008**, *3*, 210−215.
(29) Mohiuddin, T. M. G.; Lombardo, A.; Nair, R. R.; Bonetti, A.; Savini, G.; Jalil, R.; Bonini, N.; Basko, D.; Galiotis, C.; Marzari, N. Uniaxial strain in graphene by Raman spectroscopy: G peak splitting, Grüneisen parameters, and sample orientation. *Phys. Rev. B: Condens. Matter Mater. Phys.* **2009**, *79*, 205433.
(30) Lucchese, M. M.; Stavale, F.; Ferreira, E. H. M.; Vilani, C.; Moutinho, M. V. O.; Capaz, R. B.; Achete, C. A.; Jorio, A. Quantifying ion-induced defects and Raman relaxation length in graphene. *Carbon* **2010**, *48*, 1592−1597.
(31) Balandin, A. A. Thermal properties of graphene, carbon nanotubes and nanostructured carbon materials. **2011**, arXiv:1106.3789. arXiv preprint.
(32) Chen, S.; Wu, Q.; Mishra, C.; Kang, J.; Zhang, H.; Cho, K.; Cai, W.; Balandin, A. A.; Ruoff, R. S. Thermal conductivity of isotopically modified graphene. *Nat. Mater.* **2012**, *11*, 203.
(33) You, Y.; Ni, Z.; Yu, T.; Shen, Z. Edge chirality determination of graphene by Raman spectroscopy. *Appl. Phys. Lett.* **2008**, *93*, 163112.
(34) Neubeck, S.; You, Y. M.; Ni, Z. H.; Blake, P.; Shen, Z. X.; Geim, A. K.; Novoselov, K. S. Direct determination of the crystallographic orientation of graphene edges by atomic resolution imaging. *Appl. Phys. Lett.* **2010**, *97*, 053110.
(35) Krauss, B.; Nemes-Incze, P.; Skakalova, V.; Biro, L. P.; von Klitzing, K.; Smet, J. H. Raman scattering at pure graphene zigzag edges. *Nano Lett.* **2010**, *10*, 4544−4548.
(36) Yamada, Y.; Kawai, M.; Yorimitsu, H.; Otsuka, S.; Takanashi, M.; Sato, S. Carbon materials with zigzag and armchair edges. *ACS Appl. Mater. Interfaces* **2018**, *10*, 40710.
(37) Owens, F. J. Electronic and magnetic properties of armchair and zigzag graphene nanoribbons. *J. Chem. Phys.* **2008**, *128*, 194701.
(38) Merino-Díez, N.; Garcia-Lekue, A.; Carbonell-Sanromà, E.; Li, J.; Corso, M.; Colazzo, L.; Sedona, F.; Sánchez-Portal, D.; Pascual, J. I.; de Oteyza, D. G. Width-Dependent Band Gap in Armchair Graphene Nanoribbons Reveals Fermi Level Pinning on Au(111). *ACS Nano* **2017**, *11*, 11661−11668.
(39) Tang, G.; Zhang, Z.; Deng, X.; Fan, Z.; Zeng, Y.; Zhou, J. Improved scaling rules for bandgaps in graphene nanomeshs. *Carbon* **2014**, *76*, 348−356.
(40) Alajtal, A. I.; Edwards, H. G. M.; Elbagerma, M. A.; Scowen, I. J. The effect of laser wavelength on the Raman Spectra of phenanthrene, chrysene, and tetracene: Implications for extra-terrestrial detection of polyaromatic hydrocarbons. *Spectrochim. Acta, Part A* **2010**, *76*, 1−5.
(41) Yang, R.; Shi, Z.; Zhang, L.; Shi, D.; Zhang, G. Observation of RamanG-Peak Split for Graphene Nanoribbons with Hydrogen-Terminated Zigzag Edges. *Nano Lett.* **2011**, *11*, 4083−4088.

DOI: 10.1021/acsomega.8b02744
ACS Omega 2018, 3, 17789−17796

(42) Kim, J.; Yamada, Y.; Suzuki, Y.; Ciston, J.; Sato, S. Pyrolysis of epoxidized fullerenes analyzed by spectroscopies. *J. Phys. Chem. C* **2014**, *118*, 7076−7084.
(43) Frisch, M.; Trucks, G.; Schlegel, H. B.; Scuseria, G.; Robb, M.; Cheeseman, J.; Scalmani, G.; Barone, V.; Mennucci, B.; Petersson, G. *Gaussian 09*, revision D. 01; Gaussian, Inc.: Wallingford CT, 2009.

DOI: 10.1021/acsomega.8b02744
ACS Omega 2018, 3, 17789−17796